Electronic Supplementary Material (ESI) for Catalysis Science & Technology.
This journal is © The Royal Society of Chemistry 2018

Supporting Information

ZnO Nanowire Arrays Decorated with PtO Nanowires for Efficient Solar Water Splitting

Shurong Fu[a,b], Beibei Zhang[a], Hongyan Hu [a,*], Yajun Zhang[a] and Yingpu Bi [a,*]

[a]State Key Laboratory for Oxo Synthesis & Selective Oxidation, National Engineering Research Center for Fine Petrochemical Intermediates, Lanzhou Institute of Chemical Physics, CAS, Lanzhou, Gansu 730000, China. E-mail: yingpubi@licp.cas.cn

[b]University of Chinese Academy of Sciences, Beijing 100049, China.

Experimental Section

All reagents were used without any further purification.

Preparation of ZnO nanowire arrays thin films: The ZnO nanowire arrays were fabricated by the sol-gel spin coating and hydrothermal methods in our previous report[1]. Fluorine-doped tin oxide (FTO, 1.0×5.0 cm^2)-coated glass substrate were ultrasonically cleaned for 20 min with acetone, isopropanol, ethanol and deionized water, respectively. In a typical experimental procedure, 0.05 M zinc acetate dehydrate [$Zn(CH_3COO)_2 \cdot 2H_2O$] was dissolved in ethylene glycol monomethyl ether (EM) and stirred at 60 °C for 30 min. Then, an equal amount of diethanolamine (DEA) was added to the mixture to stabilize the solution and stirred at 60 °C for 2 hours. After that, the as-prepared sol was sealed and put for 2 days. Next, the precursor sol (100 μL) was spin coated over an FTO substrate using a vacuum spin coater. The sample was dried in an oven at 150 °C for 15 min and repeated the process for three times. The thin film was annealed in a muffle furnace in air at 350 °C for 30 min to remove residual solvent and obtain the ZnO seed layer. Then, the ZnO seed layer was subjected to the hydrothermal process for the growth of ZnO nanowire arrays. The coated ZnO seed substrate was immersed into the solution mixture to grow ZnO nanowire arrays at 95 °C for 6 h, which contained 0.04 M aqueous solutions of zinc nitrate [$Zn(NO_3)_2 \cdot 6H_2O$] and 0.04 M hexamethylene tetraamine (HMT). Finally, the film was washed with deionized water and absolute ethyl alcohol for several times to remove excess HMT and unreacted or non-adherent particles, followed by a drying step in an oven at 60 °C. Then, the ZnO nanowire arrays thin film was annealed in a muffle furnace in air at 550 °C for 1 h with a heating rate of 2 °C min^{-1}.

Preparation of the cross-linked PtO/ZnO nanowire arrays**:** The vertically-oriented PtO nanowires bonded ZnO nanowire arrays was fabricated by using a photo-controlled growth method. The procedure was carried out through a three electrode cell with a Pt foil as the counter electrode, the prepared sample as the working electrode and a saturated calomel electrode (SCE) as reference electrode. The ZnO nanowire arrays were immersed in 0.4 mM

H_2PtCl_6, 0.1 M Na_3PO_4 and 0.15 M polyvinylpyrrolidone (PVP) aqueous solution and then illuminated by a 300 W Xe lamp (HSX-F/UV 300) for 4 minutes under certain bias voltages. The irradiated light was full light and the power was fixed at 150 $mW \cdot cm^{-2}$. The films were then rinsed thoroughly with deionized water and dried at 60 °C in vacuum.

***Characterization*:** The crystal structures of the films were determined by X-ray diffraction (PANalytical X'Pert PRO) using graphite monochromized Cu Kα radiation (40 kV). The morphology and elemental distributions of these as-prepared products were observed by using a filed-emission scanning electron microscope (JSM-6701F, JEOL, 5kV) with an energy dispersive spectrometer (EDS). The element composition was carried out by using X-ray photoelectron spectroscope (XPS, ESCALAB 250Xi) with X-ray monochromatisation as the excitation source. The UV-vis absorption spectra were recorded on a UV-2550 (Shimadzu) spectrophotometer by using $BaSO_4$ as the reference. An F-7000 spectrofluorometer (Hitachi High-Technologies) was employed to measure the photoluminescence (PL) spectra for samples with excitation wavelength at 325 nm.

***Photoelectrochemical Measurements*:** The photoelectrochemical measurement of the photoanodes were carried out in a three-electrode configuration (photoanode as working electrode, SCE as reference electrode and Pt as counter electrode) under an air mass 1.5 (AM 1.5G, 100 $mW \cdot cm^{-2}$) illumination provided by a solar simulator. An aqueous solution of 0.2 M Na_2SO_4 was used as the electrolyte and the data was recorded by an electrochemical workstation (CHI760E). The scan rate of linear sweep voltammograms (LSV) was 10 mV s^{-1} and the scanned range was -0.4 V to +1.0 V (vs. SCE). The recorded potentials vs. SCE were converted to the reversible hydrogen electrode (RHE) scale according to the following equation: $E_{RHE}=E_{SCE}+0.059pH+E^0_{SCE}$, where E_{SCE} was the experimentally measured potential and $E^0_{SCE}=0.24$ V at room temperature. Stability measurements (current-time) were conducted at a bias voltage of 1.23 V (vs. RHE). Electrochemical impedance spectroscopy (EIS) measurements were performed by applying 0.2 V (vs. SCE) at a frequency range of 10^{-2} Hz to

10^5 Hz with small AC amplitude of 10 mV. The incident photon to current efficiency (IPCE) was measured with the aid of a monochromator (Oriel Cornerstone1301/8 m), and calculated using the following Equation 1:

$$\mathrm{IPCE}(\%) = \frac{1240 \times \mathrm{I}(\mathrm{mA/cm^2})}{\mathrm{P_{light}}(\mathrm{mW/cm^2}) \times \lambda(\mathrm{nm})} \times 100 \qquad (1)$$

Where I was the measured photocurrent density at a specific wavelength, λ was the wavelength of incident light and $\mathrm{P_{light}}$ was the measured light power density at that wavelength.

Using Ar as a carrier gas, the evolved amounts of H_2 and O_2 from the PEC cell system were analyzed by a gas chromatograph equipped with a thermal conductivity detector (TCD). Light source and electrolyte were the same as these used for above PEC measurements. According to the standard H_2 and O_2 evolution curve, the amount of generated H_2 and O_2 were measured by taking 0.5 mL gas products using a syringe and injecting it into the gas-sampling loop every 10 min at a constant potential of 0.6 V (vs. SCE).

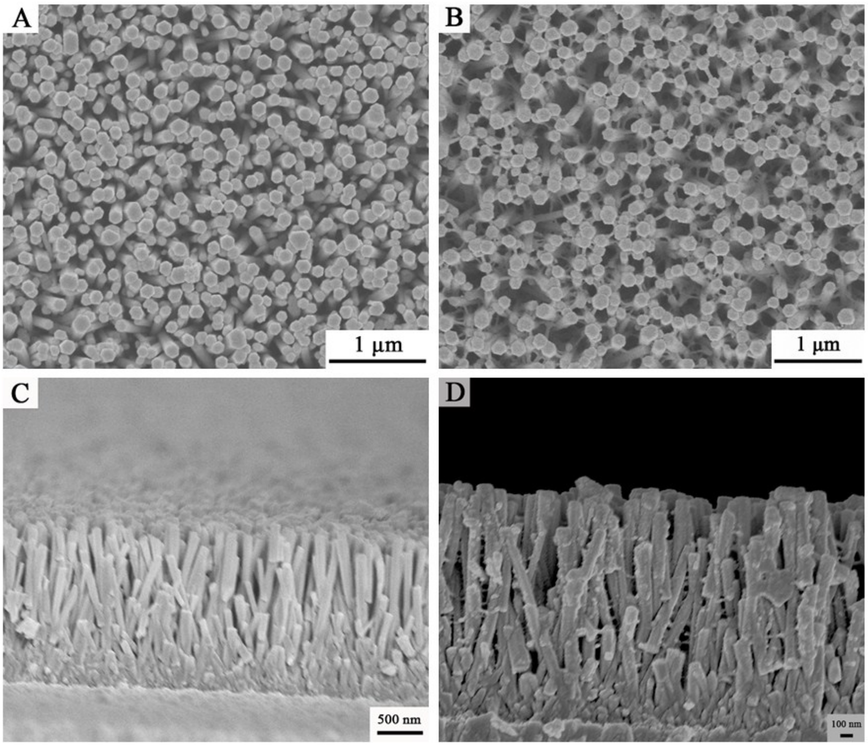

Fig. S1 (A, C) Top-view and cross-section SEM images of pure ZnO nanowire arrays; (B, D) Top-view and cross-section SEM images of cross-linked PtO/ZnO nanowire arrays.

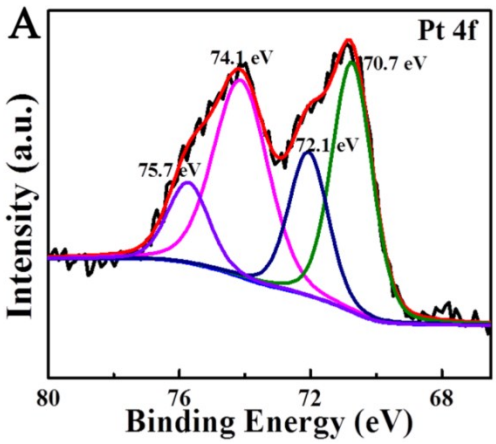

Fig. S2 The XPS spectra of Pt 4f for cross-linked PtO/ZnO nanowire arrays reduced by $NaBH_4$ (2 mg/mL) for 40 min (A) and 120 min (B).

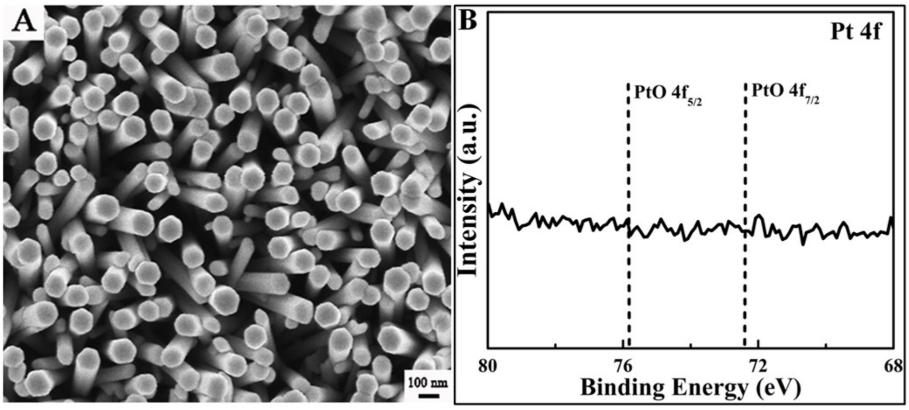

Fig. S3 SEM images (A) and XPS spectra (B) of the PtO/ZnO composites without Xe lamp illumination in the growth process.

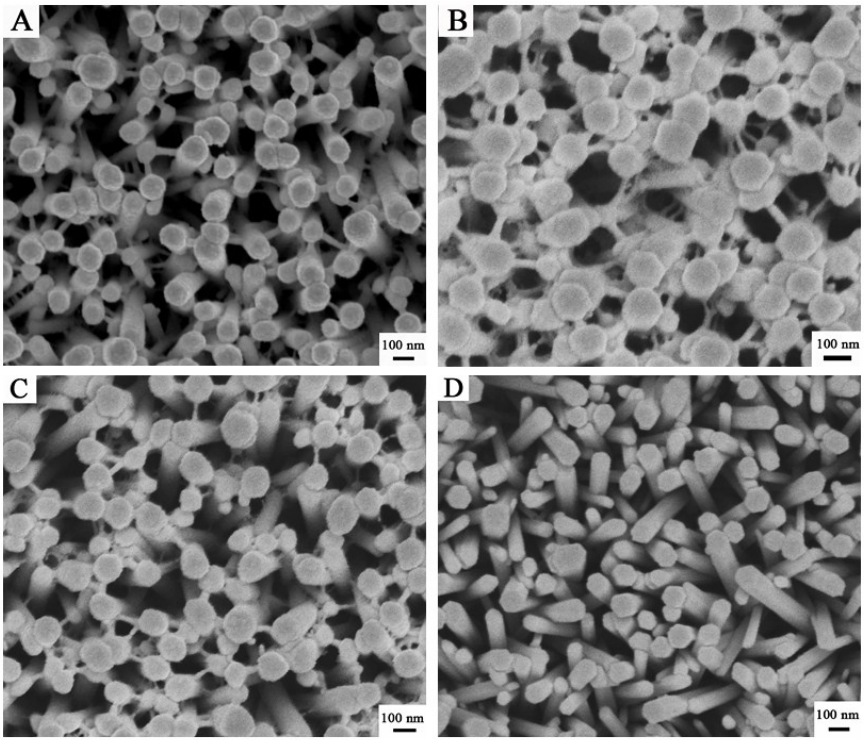

Fig. S4 (A) SEM images of cross-linked PtO/ZnO nanowire arrays synthesized at 0.2 V (A), 0.6 V (B), 1.2 V (C) and 1.6 V (D) vs. SCE.

Results and discussion:

The compositions and structures of the cross-linking 3D hetero-nanostructures could be rationally tuned by adjusting the experimental parameters. The as-prepared PtO-ZnO nanowire arrays at different bias voltages were presented in Fig. S4A, B, C and D. It revealed that the formation and the amount of PtO nanowires were related to the bias voltage. When the bias voltage increased from 0.2 V to 0.6 V, the amount of PtO nanowires was increased. While the amount of PtO nanowires was decreased or even disappeared with the bias voltage further increased up to 1.2 V and 1.6 V.

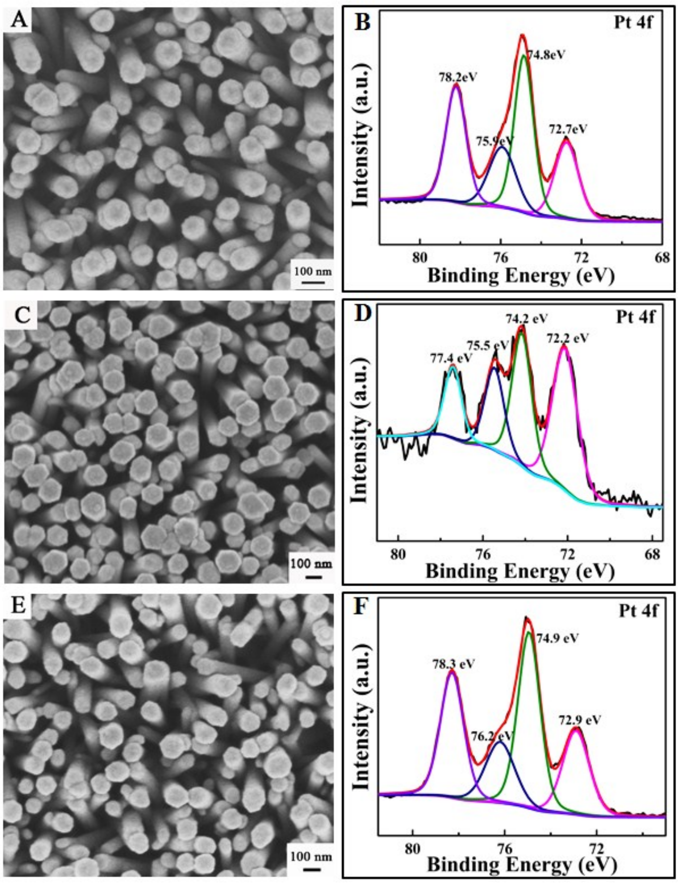

Fig. S5 SEM images and XPS spectra of PtO/ZnO nanowire arrays reacted in 0.4 mM H_2PtCl_6 and 0.15 M PVP (A, B), 0.4 mM H_2PtCl_6 and 0.1 M Na_3PO_4 (C, D), and only 0.4 mM H_2PtCl_6 aqueous solution (E, F), respectively.

Results and discussion:

Furthermore, the comparison experiments were designed to elucidate the effect of Na_3PO_4 and PVP on the morphology variety of as-prepared PtO/ZnO heterostructures. As shown in Fig. S5, in the absence of Na_3PO_4 or PVP or both, it clearly observed that no PtO nanowires were formed among ZnO nanowire arrays. Moreover, the corresponding high resolution XPS spectra of Pt 4f (Fig. S5B, D and F) showed that the surface Pt species of PtO/ZnO heterostructures were Pt^{2+} (PtO) and Pt^{4+} (PtO_2).

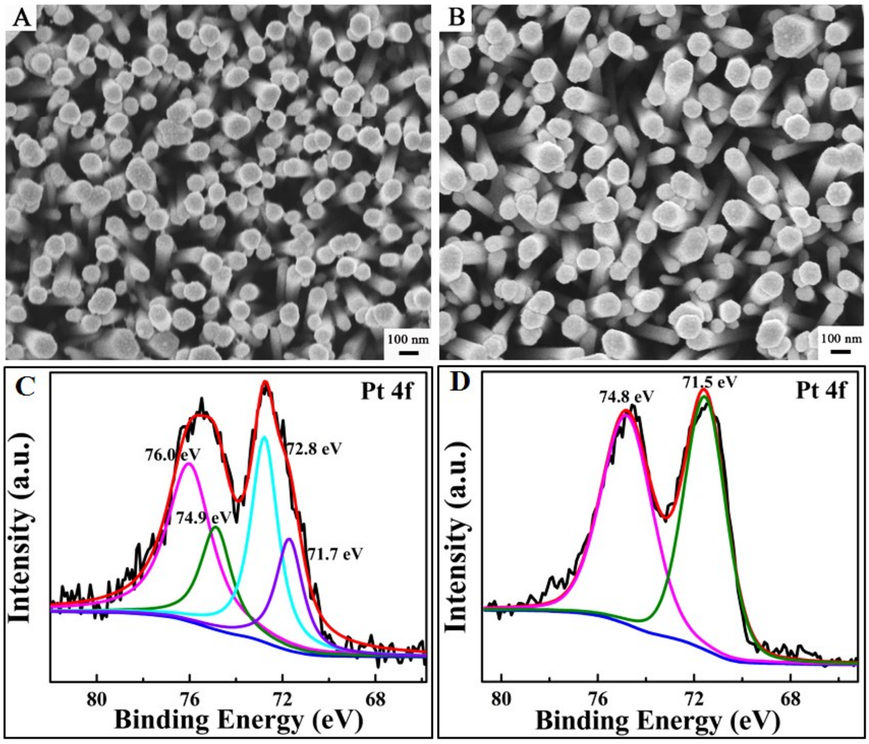

Fig. S6 SEM images and XPS spectra of PtO/ZnO nanowire arrays reacted in 0.4 mM H_2PtCl_6, 0.1 M Na_3PO_4, 0.15 M PVP and 2 mg $NaBH_4$ (A, C), 0.4 mM H_2PtCl_6, 0.1 M Na_3PO_4, 0.15 M PVP and 10 mg $NaBH_4$ (B, D), respectively.

Results and discussion:

In addition, when the $NaBH_4$ (2 mg) was added into the reaction solution in the photo-controlled process, a small amount of PtO nanowires and Pt^0 were formed (Fig. S6A, C). Further increasing the amount of $NaBH_4$ to 10 mg, no PtO nanowires were formed and the Pt species was only Pt^0 (Fig. S6B, D). Therefore, the strength of the reducing agent (PVP) determined the chemical state of the surface Pt species and the formation of PtO nanowires under the photoassisted electrochemical deposition reaction process.

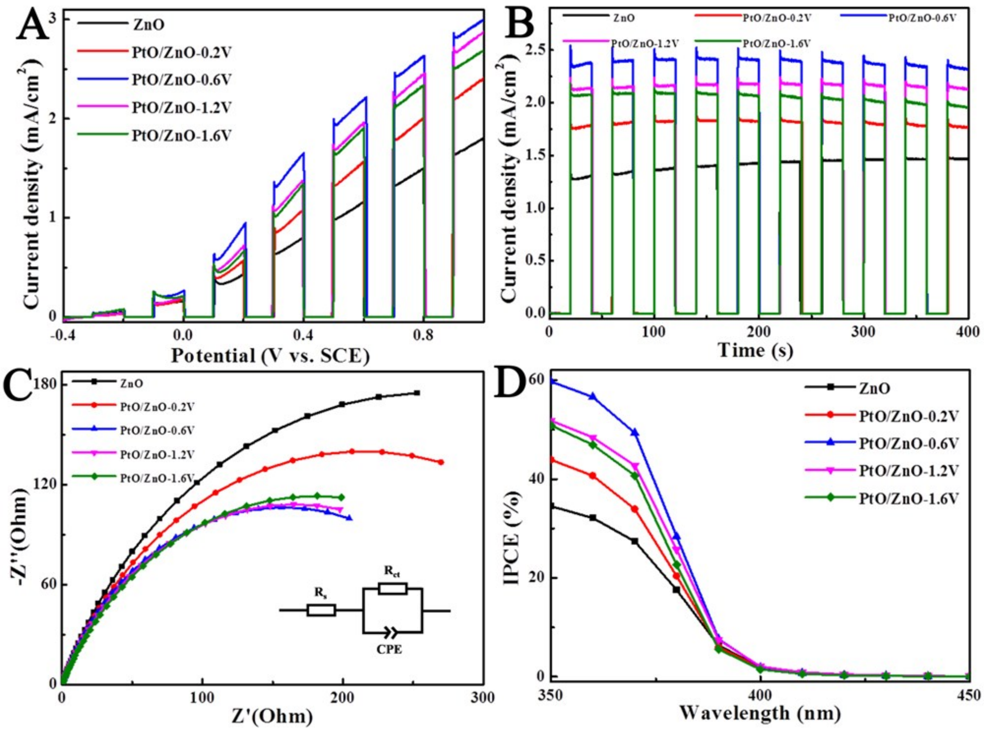

Fig. S7 (A) The LSVs, (B) amperometric i-t curves at 0.6 V vs. SCE, (C) EIS curves, and (D) IPCE spectra for pure ZnO nanowire arrays and cross-linked PtO/ZnO nanowire arrays under AM 1.5G illumination. Measurements were conducted in an electrolyte of 0.2 mol L^{-1} Na_2SO_4 solution.

Results and discussion:

The PEC activities for water oxidation of photoanodes synthesized at different bias voltages were examined by measuring the photocurrent density versus bias potential (*J-V*) curves in 0.2 M Na_2SO_4 electrolyte under AM 1.5 G irradiation (100 mW·cm^{-2}). As shown in Fig. S7A and 7B, the photocurrent density of the ZnO nanowire arrays remarkably enhanced after the modification with PtO nanostructures (nanowires and nanoparticles). Moreover, it can be seen that the photocurrent density of the cross-linked PtO-ZnO nanowire arrays could be further enhanced with increasing the amount of PtO nanowires. The photocurrent density of the cross-linked PtO-ZnO nanowire arrays synthesized at 0.6 V was the highest. These phenomenon confirmed the positive effects of PtO nanostructures and the efficient charge separation between ZnO and PtO. In addition, Fig. S7C showed EIS curves for ZnO and cross-linked PtO/ZnO nanowire arrays to study the charge transfer at the interface of the electrode/electrolyte. The arch in the Nyquist plot represents the charge transfer kinetics on the working electrode as the diameter of the semicircle reflects the charge transfer resistance. The arc radius of cross-linked PtO/ZnO composite synthesized at 0.6 V was the smallest, which implied that it had the smallest charge transfer resistance and the highest charge separation efficiency. Moreover, the impedance arc radius of all cross-linked PtO/ZnO nanowire arrays were smaller than that of pure ZnO nanowire arrays, which may be attributed to the deposited PtO reducing the recombination of electron-hole pairs and accounting for the higher photocurrent response. Furthermore, the IPCE was measured to evaluate the light conversion efficiency of our electrodes in Fig. S7D. IPCE analysis of the photoanods showed a similar distribution compared with current-potential characteristics. All cross-linked PtO/ZnO nanowire arrays presented enhanced IPCE over the entire absorption region in comparison with the pure ZnO nanowire arrays, and the PtO/ZnO composites synthesized at 0.6 V exhibited the highest IPCE values. Based on these results, we rationally speculate that the PtO nanowires as cocatalyst can accelerate hole output from electrode to electrolyte for fast water oxidation reaction, reducing the accumulated surface holes of ZnO and increasing the photocurrent.

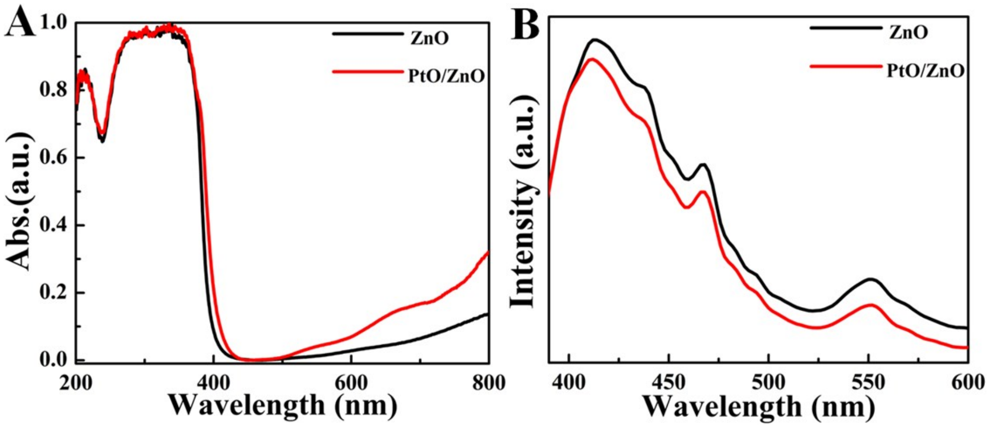

Fig. S8 (A) UV-vis diffuse reflectance spectra of pure ZnO and cross-linked PtO/ZnO nanowire arrays, (B) PL spectra of pure ZnO and cross-linked PtO/ZnO nanowire arrays excited at the wavelength of 325 nm.

Results and discussion:

The UV-vis absorption spectra and PL spectra of pure ZnO and the cross-linked PtO/ZnO nanowire arrays were further explored. It can be noted that PtO/ZnO composites showed the similar absorption edge with pure ZnO (Fig. S8A) and the PL intensity of ZnO was reduced after the formation of the cross-linked PtO/ZnO composite materials (Fig. S8B), which meaned that PtO could suppress the recombination process of photo-generated carriers in ZnO[2] nanowire arrays.

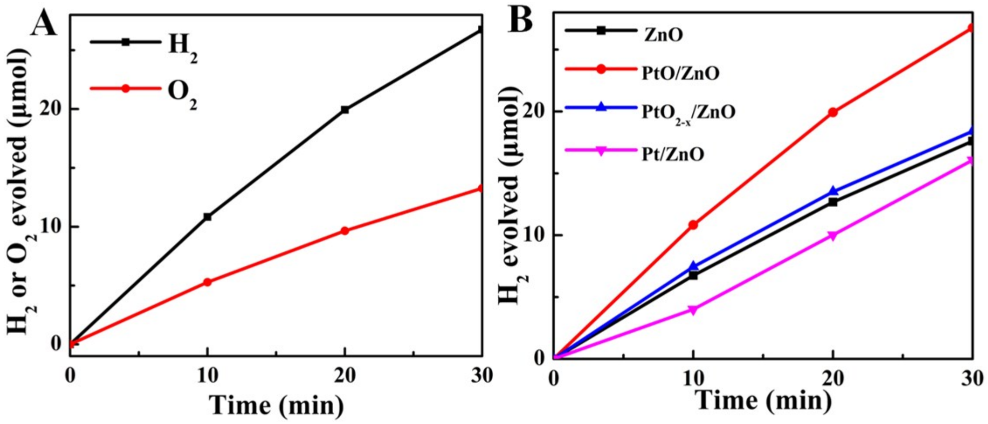

Fig. S9 The detection of H_2 and O_2 for PtO/ZnO nanowire arrays (A), H_2 evolution for different photoanodes (B) at a bias of 0.6 V under AM 1.5 G illumination in 0.2 mol L^{-1} Na_2SO_4 solution.

Results and discussion:

Fig. S9 showed the hydrogen evolution amounts versus time at the Pt counter electrode over the PtO/ZnO photoanode in 0.2 M Na_2SO_4 electrolyte and applied bias voltage (1.23 V_{RHE}) under AM 1.5G illumination, and H_2 generation was detected with Gas Chromatography (GC). It can be clearly seen that the amount of H_2 and O_2 were linearly related to the reaction time during the water splitting process, and the stoichiometric ratio of H_2 to O_2 evolution was approximately kept at 2:1. With prolonged light irradiation time up to 30 min, the amount of H_2 and O_2 has been increased up to 26.8 and 13.5 μmol, respectively, indicating that the stable PEC water splitting into hydrogen and oxygen gas has been achieved for the cross-linked PtO/ZnO nanoarray photoanodes. In addition, the amounts of H_2 evolution of the PtO_{2-x}/ZnO, Pt/ZnO, and pure ZnO nanowire arrays have also been measured under the same conditions. It can be clearly seen from Fig. S9B that PtO/ZnO nanoarray exhibits much higher amount of H_2 evolution than PtO_{2-x}/ZnO (18.4 μmol), Pt/ZnO (16.1 μmol), and pure ZnO (17.6 μmol) nanowire arrays. Thereby, these demonstrations clearly reveal that the PtO nanowires could serve as an excellent OER cocatalyst owning to the simultaneous promoting surface charge separation and facilitating water oxidation reaction.

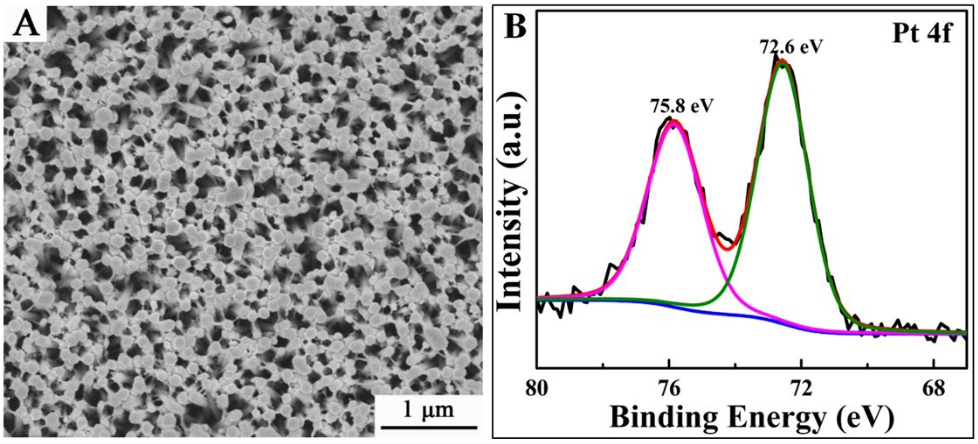

Fig. S10 SEM images (A) and the XPS spectra of Pt 4f (B) for cross-linked PtO/ZnO nanowire arrays after measured PEC.

Results and discussion:

Since the PtO could be oxidized into PtO_2 or reduced into metallic Pt, the cross-linked PtO/ZnO photoanode after PEC water splitting has been further measured by SEM and XPS. As shown in Fig. S10A, no evident change could be observed after PEC process and the PtO/ZnO nanoarray generally kept its original cross-linked structures. Moreover, the two peaks of Pt 4f at 75.8 eV and 72.6 eV could also be assigned to Pt^{2+} (Fig. S10B), indicating that PtO nanowires have not been oxidized or reduced into other Pt species, such as PtO_2 or metallic Pt. These results clearly reveal that PtO/ZnO nanoarray possesses valence state as well as structure stability for PEC water splitting.

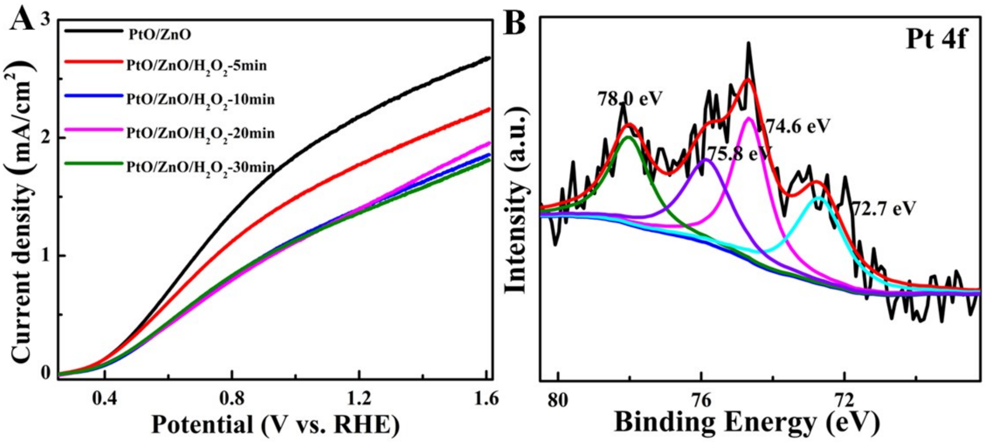

Fig. S11 *J-V* curves (A) and the XPS spectra of Pt 4f (B) for the cross-linked PtO/ZnO nanowire arrays treated with H_2O_2.

Results and discussion:

We introduced a facile and simple in situ oxidation method to further explore the effects of Pt^{2+} (PtO) species on the PEC performances. Fig. S11A shows the LSV curves of the cross-linked PtO/ZnO photoanode treated with H_2O_2 at different times. It was obviously that the photocurrent density was remarkedly decreased, which could be attributed to the partial transfrom of Pt^{2+} of PtO nanowires into Pt^{4+}. Furthermore, the corresponding XPS spectra of cross-linked PtO/ZnO photoanode were shown in Fig. S11B, indicating that the two peaks at 78.0 eV and 74.6 eV were assigned to Pt^{4+} and the other two peaks located at 75.8 eV and 72.7 eV were ascribed to Pt^{2+}. These results clearly demonstrated that PtO was more beneficial to facilitate the charge separation for improving the photocurrent density and output the photogenerated holes than that of PtO_2.

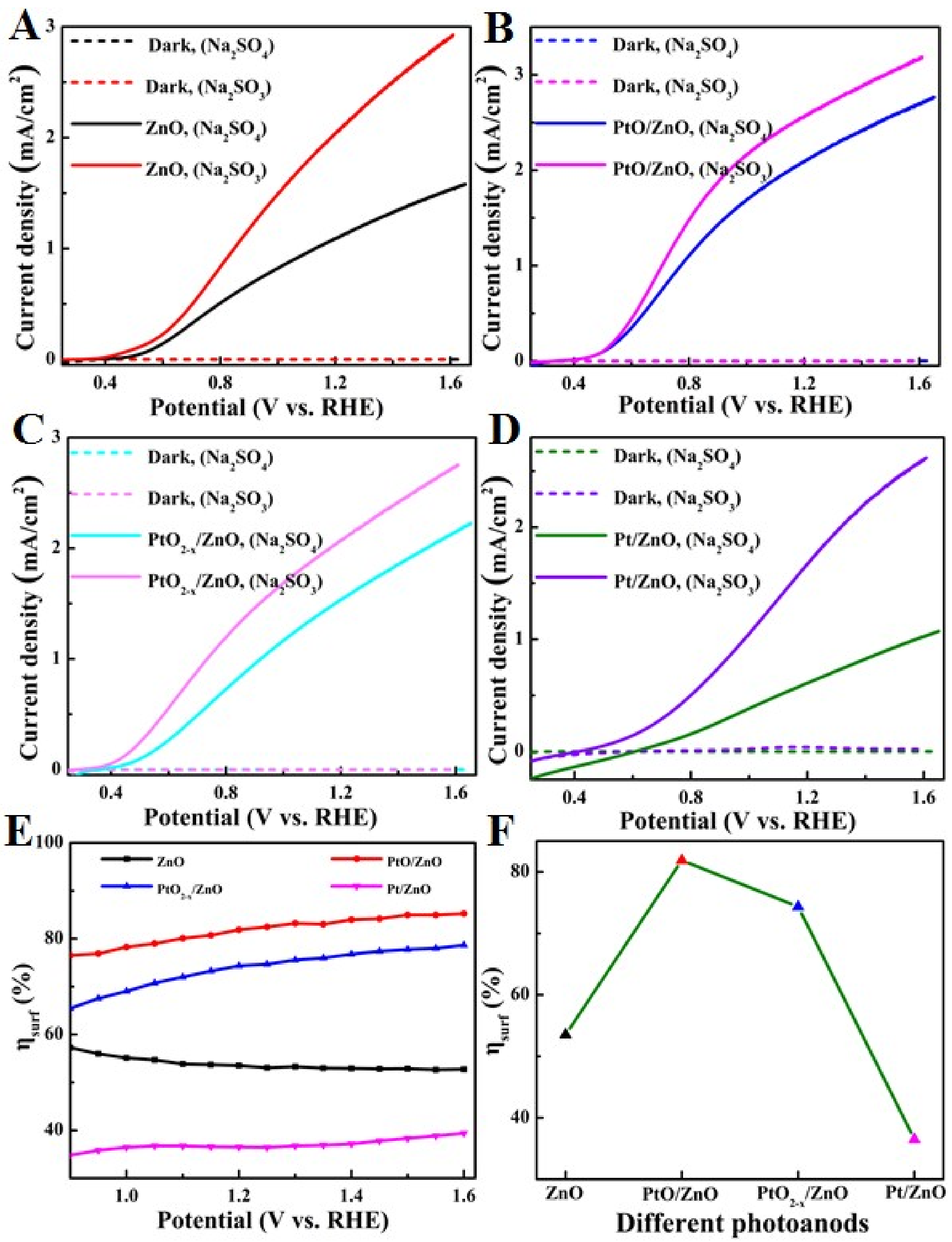

Fig. S12 *J-V* curves for the (A) pure ZnO, (B) PtO/ZnO, (C) PtO_{2-x}/ZnO and (D) Pt/ZnO photoanodes measured with and without Na_2SO_3 in the electrolyte; surface charge separation efficiency (E) and the value at 1.2 V vs. RHE (F) for the bare ZnO and different Pt species modified ZnO nanowire arrays photoanodes.

Results and discussion:

Surface charge separation efficiencies (η_{surf}) for pure ZnO and different Pt species modified ZnO nanowire arrays photoanodes were further investigated to understand the water oxidation kinetics of these photoanodes. Since the oxidation kinetics of Na_2SO_3 is very fast, the interfacial charge separation efficiency is nearly equal to 100%. Therefore, Na_2SO_3 was added into the electrolyte as a hole scavenger to evaluate the photogenerated holes at the electrode/electrolyte interface. The η_{surf} can be calculated by the Equation 2:

$$\eta_{surf} = J_{Na_2SO_4} / J_{Na_2SO_3} \qquad (2)$$

Where $J_{Na_2SO_3}$ is the phtocurrent density for Na_2SO_3 oxidation (Fig. S12A, B, C, D). The calculated efficiency in Fig. S12E revealed that η_{surf} for the vertically-oriented PtO nanowires modified ZnO photoanode (81.8% at 1.2 V_{RHE}) was about 1.5 times higher than that of pure ZnO (53.5% at 1.2 V_{RHE}). It indicated that the surface charge separation could be greatly promoted by PtO nanowires. However, when partial PtO was replaced by PtO_2, the η_{surf} value of PtO_{2-x}/ZnO was rapidly decreased down to 74.3% at 1.2 V_{RHE}, clearly confirming the relatively poor ability of surface charge separation of PtO_2 compared with PtO. In the case of Pt/ZnO photoanodes, the lowest surface charge separation efficiency (36.5% at 1.2 V_{RHE}), even lower than pure ZnO photoanodes, was obtained, which implied that metallic Pt not promote the surface charge separation, but increase the electron-hole recombination.

Notes and references

1 T. Wang, B. Jin, Z. Jiao, G. Lu, J. Ye and Y. Bi, *Chem. Commun.* **2015**, 51, 2103-2106.

2 S. J. A. Moniz, J. Zhu, J. Tang, *Adv. Energy Mater.* **2014**, 4, 1301590-1301597.